ACS APPLIED MATERIALS & INTERFACES

Research Article

www.acsami.org

Novel Mesoporous Graphite Carbon Nitride/BiOI Heterojunction for Enhancing Photocatalytic Performance Under Visible-Light Irradiation

Chun Chang,[†,‡] Lingyan Zhu,*[,†] Shanfeng Wang,[†] Xiaolong Chu,[†] and Longfei Yue[†]

[†]Key Laboratory of Pollution Processes and Environmental Criteria, Ministry of Education, Tianjin Key Laboratory of Environmental Remediation and Pollution Control, College of Environmental Science and Engineering, Nankai University, Tianjin 300071, P.R. China

[‡]College of Chemistry, Chemical Engineering and Food Safety, Bohai University, Jinzhou 121013, Liaoning, P.R. China

Supporting Information

ABSTRACT: A novel organic−inorganic three-dimensional (3D) mesoporous graphite carbon nitride/BiOI (MCN/BiOI) heterojunction photocatalyst with excellent visible-light-driven photocatalytic performance was synthesized by a facile solvothermal method and used for degradation of bisphenol A (BPA) in water. After hybridization with MCN, a heterojunction was formed and the photogenerated carriers could be effectively separated by the internal electric field built at the heterojunction interface. The photocatalytic and photoelectrochemical performance of BiOI were improved and much higher than pure BiOI and MCN. The best photocatalytic performance was achieved with MCN proportion of 10%, and the k_{obs} was approximately 1.6 times of pure BiOI and 3.4 times of MCN under simulated solar light irradiation, respectively. The photocurrent intensity generated by 10%-MCN/BiOI electrode was about 1.5 and 2.0 times of those induced by BiOI and MCN under visible-light irradiation, respectively. The superoxide radical species were predominant in the reaction system.

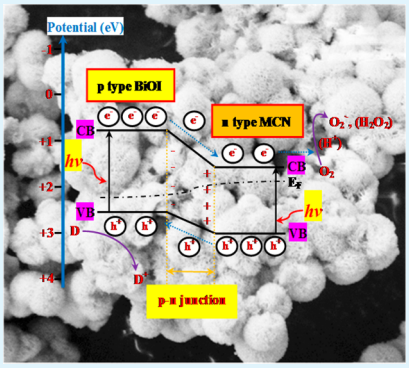

KEYWORDS: *n-type MCN/p-type BiOI heterojunction, organic−inorganic hybrid photocatalyst, photocatalysis mechanism*

1. INTRODUCTION

Environmental pollution and fossil energy shortage are two of the biggest challenges in the present world. Photocatalysis using semiconductors is one of the promising technologies to achieve efficient pollution remediation and clean hydrogen energy supplies. TiO_2 is very effective in photocatalytic degradation of pollutants and hydrogen production. However, the application of TiO_2 is severely restricted due to its wide bandgap, which could only be excited by UV light less than 387.5 nm and high recombination of photogenerated hole-electron pairs.[1] It is important to exploit new photocatalysts with strong photoresponse in wide wavelength and high efficient charge separation. Bismuth oxyhalides (BiOX, X = Cl, Br, I) are an emerging family of promising photocatalysts which exhibit excellent photocatalytic performance because of their layered tetragonal crystal structure and suitable band gaps.[2] Among them, BiOI is an attractive p-type semiconductor,[3] and displays the greatest absorption in the visible light region as a result of its smallest band gap (1.7−1.8 eV) comparing with other bismuth oxyhalides (BiOX, X = Cl, Br).[4] To exploit its application in water treatment, much concern has been raised to improve the photocatalytic performance of BiOI by hybridizing it with other semiconductors to facilitate photoinduced electron-hole separation. Until now, BiOI-based heterojunctions coupling with other inorganic semiconductors, such as TiO_2/BiOI,[5] ZnO/BiOI,[6] Bi_2S_3/BiOI,[2] Bi_2WO_6/BiOI,[7] AgI/BiOI,[8] etc., have been successfully synthesized and they display improved photocatalytic efficiency as compared to pure BiOI.

In recent years, metal-free polymeric graphitic-like carbon nitride (g-C_3N_4) has attracted considerable attention due to its specific electronic properties and thermal and chemical stability.[9,10] Wang et al. firstly reported that g-C_3N_4 displayed good visible-light-driven photocatalytic performance and can produce hydrogen or oxygen by water splitting under visible light.[11] On the basis of this, mesoporous g-C_3N_4 (MCN) has been synthesized and displays much higher H_2 evolution activity than bulk g-C_3N_4.[12] To further improve the photoactivity of MCN, researchers have developed several techniques, including morphology control (from nanoplates to nanorods),[13] doping with nonmetallic elements (B,[14,15] F,[14,16] P,[17] and S[18,19]), deposition with metal atoms (Fe,[20,21] Mn; Co; Ni; Cu,[22] Pd,[23] Pt,[24] and Au[25]), and coupling with inorganic semiconductors (TiO_2,[26] ZnO,[27,28] NiS,[29] $ZnWO_4$,[30,31] Bi_2WO_6,[32,33] $BiPO_4$,[1] Ag_3PO_4[10]).

Received: January 13, 2014
Accepted: March 17, 2014
Published: March 17, 2014

   dx.doi.org/10.1021/am5002597 | ACS Appl. Mater. Interfaces 2014, 6, 5083−5093

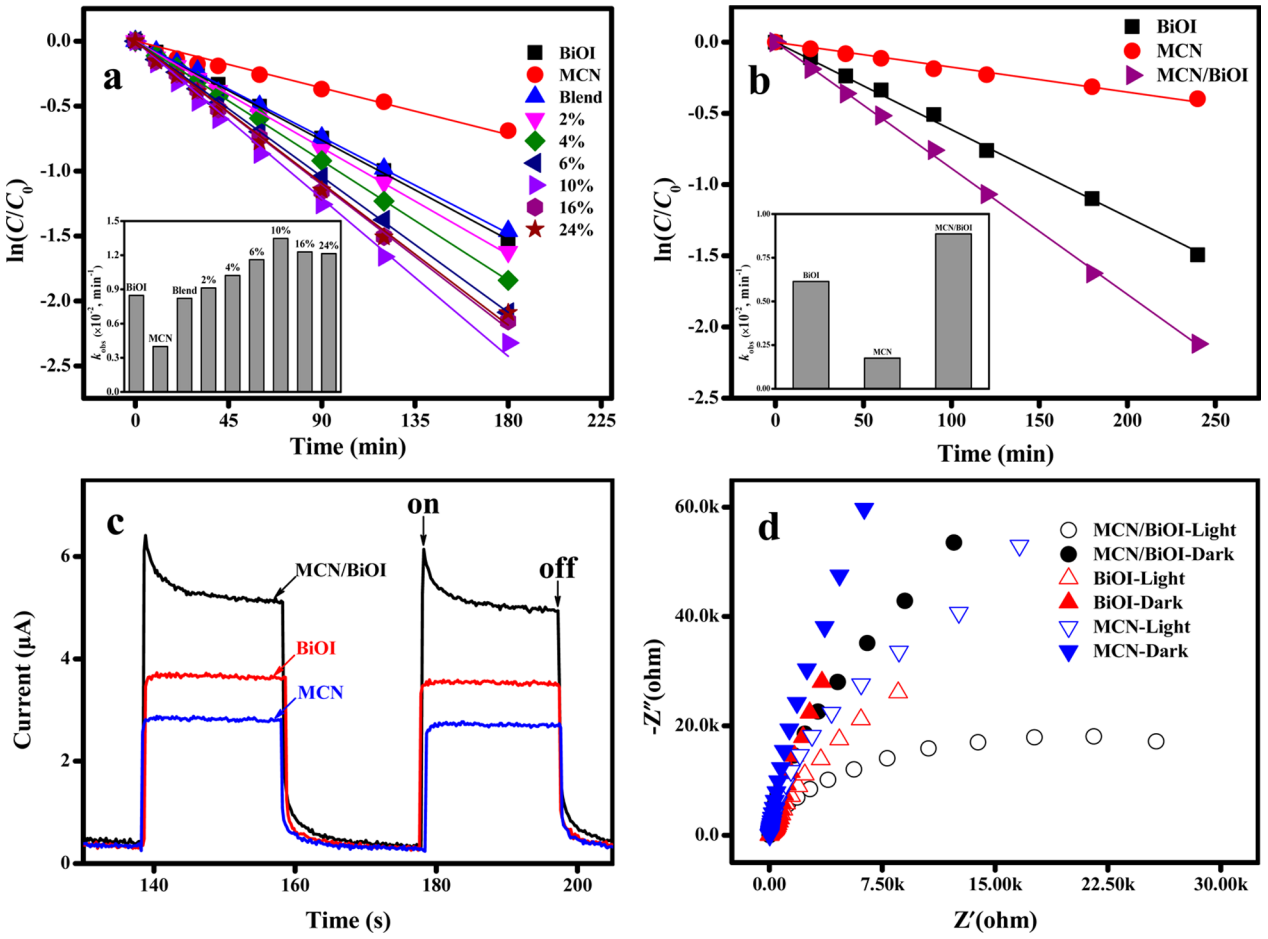

Figure 1. Photocatalytic degradation of BPA by BiOI, MCN, and MCN/BiOI (photocatalysts, 1.0 g/L; BPA initial concentration, 20 mg/L; pH 6.28): (a) under simulated solar light irradiation (λ > 290 nm); (b) under visible light irradiation (λ > 400 nm); (c) photocurrent responses; and (d) EIS Nyquist plots of MCN, BiOI, and 10%-MCN/BiOI (λ > 400 nm).

Fu et al. synthesized a BiOBr-C_3N_4 heterojunction by depositing BiOBr nanoflakes onto the surface of C_3N_4, which displayed enhanced photocatalytic degradation efficiency to Rhodamine B as compared to pure BiOBr and C_3N_4.[34] However, the low- dimensional nanoscaled materials tend to aggregate during synthesis, resulting in a reduction of surface area and photocatalytic performance.[35] 3D hierarchical heterojunction materials have a high surface-to-volume ratio, and are considered favorable for photocatalytic performance.[36] It is hypothesized that 3D p−n heterojunction of BiOI and MCN would give rise to an inorganic−organic composite with good visible-light absorption and efficient photocatalytic performance.

Herein, the primary objective of current study was to synthesize novel 3D MCN/BiOI heterojunction photocatalysts by a facile solvothermal method. The resultant photocatalysts were characterized comprehensively by means of XRD, FE-SEM, HR-TEM, XPS, N_2 adsorption/desorption, UV−vis DRS, FT-IR, and so on. The photocatalytic performances of the composites were evaluated by photocatalytic degradation of bisphenol A (BPA), which is regarded as a representative endocrine disrupting chemical, and photoelectrochemical test, respectively. The interaction between MCN and BiOI as well as the photocatalytic mechanisms were investigated and discussed systematically. The reusability of the composites was also investigated.

2. EXPERIMENTAL SECTION

2.1. Synthesis and Characterization of Photocatalysts. The MCN was synthesized as reported previously with a few modifications.[37] The detailed procedure was given in Supporting Information. MCN/BiOI was synthesized by a conventional solvothermal method. Twenty milliliters of 0.15 mol L^{-1} (1.4553 g) $Bi(NO_3)_3{\cdot}5H_2O$ dissolved in glycol was drop-wisely added in the same volume of 0.15 mol L^{-1} (0.4980 g) KI which was dissolved in glycol. Then, a certain amount (0.02, 0.04, 0.06, 0.10, 0.16, 0.24 g) of MCN was added in the above mixed solution. The mixture was vigorously stirred at room temperature for 60 min and was transferred to a 50 mL of Teflon-lined autoclave, which was sealed in a stainless steel tank and maintained at 140 °C for 24 h. The autoclaves were cooled to room-temperature naturally. The solid products were washed three times with deionized water and ethanol respectively, and dried at 80 °C in oven for overnight. The nominated mass ratio of MCN to BiOI (x%) of the as-prepared composites was 2, 4, 6, 10, 16, and 24%, respectively. The resultant products were then referred as x%-MCN/BiOI.

The prepared samples were characterized by means of FE-SEM, HR-TEM, XRD, XPS, FT-IR, UV−vis DRS, and N_2 adsorption/desorption. The detailed information about the characterization methods is provided in the Supporting Information.

2.2. Photoelectrochemical Measurement. Photoelectrochemical test with an Autolab PGSTAT302N electrochemical system (Metrohm Ltd., Switzerland) was carried out in a conventional three-electrodes, a single-compartment quart cell filled with 0.1 M Na_2SO_4 electrolyte and a potentiostat. The ITO/photocatalyst electrode served as the working electrode. A platinum wire was used as a counter

dx.doi.org/10.1021/am5002597 | ACS Appl. Mater. Interfaces 2014, 6, 5083−5093

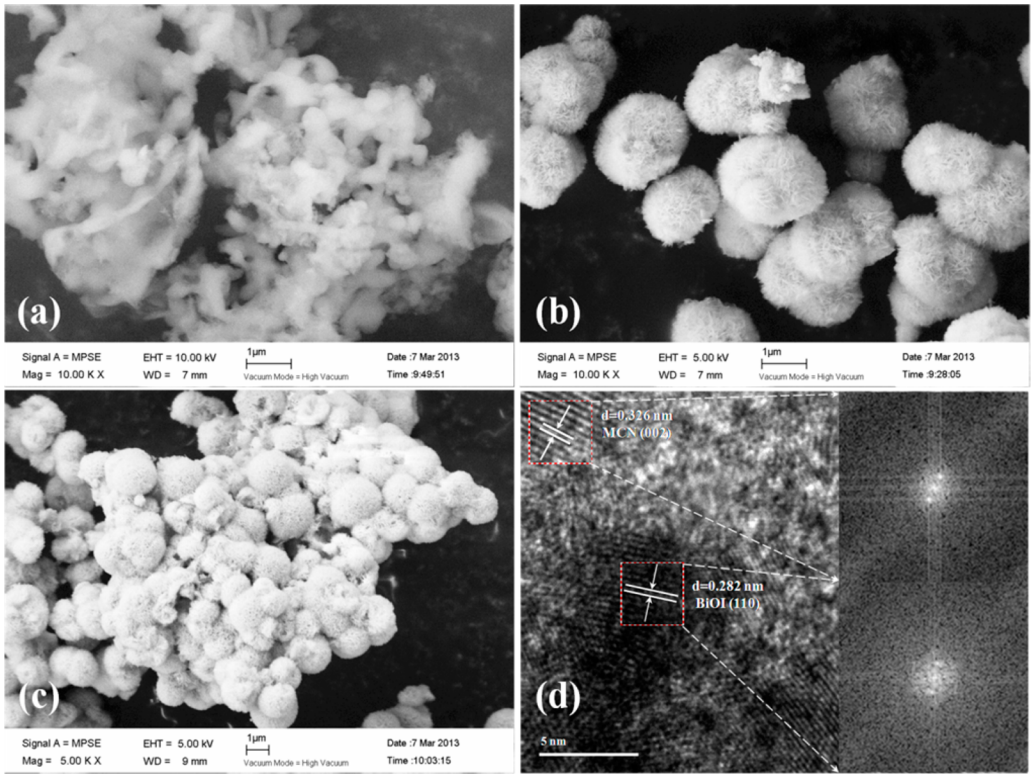

Figure 2. SEM images of (a) MCN and (b) BiOI; (c) SEM and (d) HRTEM (inset, FFT pattern) of 10%-MCN/BiOI.

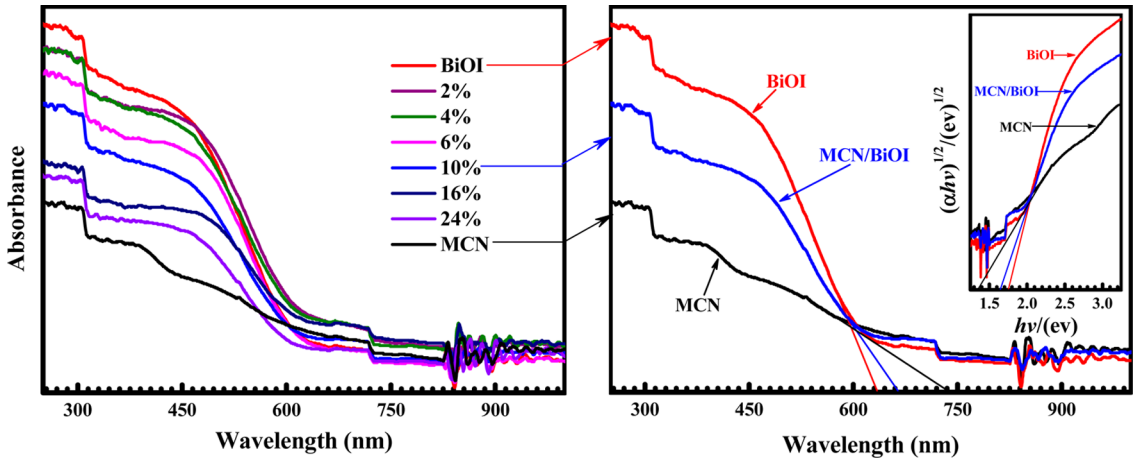

Figure 3. UV−vis diffuse reflection spectra of the prepared materials (inset at left corner: the band gaps of the MCN, BiOI, and 10%-MCN/BiOI).

electrode with Ag/AgCl (saturates KCl) as a reference electrode. The photoreponses of the photocatalysts were measured at 0.0 V as visible light (λ > 400 nm) was switched on and off. Electrochemical impedance spectra (EIS) were recorded at 0.0 V. A sinusoidal ac perturbation of 10 mV was applied to the electrode over the frequency range of 0.01 to 1 × 10^4 HZ.

2.3. Degradation Experiments. Batch experiments were conducted in a XPA-7 photochemical reactor (Xujiang Electromechanical plant, Nanjing, China) to investigate the photocatalytic performanc of the prepared materials. Simulated solar light and visible light irradiation was provided by a 350 W xenon lamp (λ > 290 nm Institute of Electric Light Source, Beijing) without/with a 400 nm cutoff filter, respectively, and light intensity of 5.8 mW cm^{-2}, the emission spectrum of the lamp is shown in Figure S1 in the Supporting Information. The reaction system was cooled by circulating water and maintained at room temperature. In quartz test tubes, 0.0100 g of catalysts were added followed by adding 10 mL of BPA aqueous solution at 20 mg L^{-1}. The solution was magnetically stirred during the reaction. Before irradiation, the suspension was stirred in the dark for 45 min to establish adsorption−desorption equilibrium of BPA on the catalysts. Approximately 0.6 mL of aqueous sample was withdrawn at certain time intervals and centrifuged under 8000 rpm before the analysis. Detailed information is given in the Supporting Information.

3. RESULTS AND DISCUSSION

3.1. Photocatalytic and Photoelectrochemical Performance. Panels a and b in Figure 1 compare the photocatalytic performance of pure BiOI, MCN, and their hybridized composites to degrade BPA under simulated solar light and visible-light irradiation, respectively. The following pseudo first-order reaction kinetic model might be used to describe the degradation reaction process:

dx.doi.org/10.1021/am5002597 | ACS Appl. Mater. Interfaces 2014, 6, 5083−5093

Table 1

(a) Pearson Absolute Electronegativity (PAE) of Constituent Atoms of the Photocatalysts					
	C	N	Bi	O	I
PAE	6.27	7.30	4.69	7.54	6.76
(b) Energy Band Structure Parameters of MCN, BiOI, and MCN/BiOI					
photocatalysts	E_g (eV)	X (eV)	E_{VB} (eV)	E_{CB} (eV)	
MCN	1.38	6.84	3.03	1.65	
BiOI	1.75	6.21	2.58	0.83	

$$\ln(C_{BPA,t}/C_{BPA,0}) = -k_{obs}t \quad (1)$$

where $C_{BPA,t}$ is the concentration of BPA in aqueous phase (mg L^{-1}), $C_{BPA,0}$ is the initial concentration of BPA (mg L^{-1}), k_{obs} is the pseudo first-order rate constant (min^{-1}), and t is the reaction time (min). The pseudo first-order reaction kinetic model fitted the experimental data very well with regression coefficient $R^2 > 0.9867$ in all cases. The reaction rate constants k_{obs} were calculated from the corresponding slope of the fitting line, and are shown in Figure 1 (inset). Figure 1a demonstrates that all of the MCN/BiOI composites exhibited higher photocatalytic performance than pure MCN and BiOI under simulated solar light irradiation. The photocatalytic performance was enhanced gradually with increasing the proportion of MCN. The maximum k_{obs} (0.0135 min^{-1}) was achieved with 10% of MCN in the composite, and it was approximately 1.6 times of pure BiOI (0.0085 min^{-1}) and 3.4 times of MCN (0.0040 min^{-1}) under the same conditions. This could be explained by the effective separation of photogenerated hole-electron pairs due to the formation of heterojunctions between MCN and BiOI in the composite. However, as the proportion of MCN further increased, the degradation rate decreased gradually, though it was still higher that of pure BiOI. Although MCN is favorable for separation of photogenerated hole-electron pairs, more MCN in the composite might reduce the photoabsorption of visible light. As a result, the photocatalytic performance of MCN/BiOI decreased as the proportion of MCN further increased. Similar results were also reported for C_3N_4/ZnO,[27] C_3N_4/Zn_2WO_4,[31] and C_3N_4/Bi_2WO_6.[33] Compared with pure BiOI, the mechanical mixture of MCN (10%) and BiOI did not show any increase in the catalytic performance, suggesting that the close interaction between MCN and BiOI in the hybridized composite might promote the charge separation, and enhance the photocatalytic performance.

The photocatalytic performance of BiOI hybridized with MCN was also investigated under visible light irradiation, and the results are shown in Figure 1b. Similar to the results with simulated solar light irradiation, the 10%-MCN/BiOI also displayed the highest photocatalytic performance, which is much higher than that of pure MCN and BiOI. Almost 90.0% of BPA at 20 mg L^{-1} was photodegraded by 1.0 g L^{-1} 10%-MCN/BiOI after irradiation with visible light for 4 h, whereas the removal rates of pure MCN and BiOI were 34.0 and 78.7%, respectively.

The photoeletrochemical performance could be investigated by photocurrent response and EIS.[27] The photoresponses of ITO/MCN, ITO/BiOI, and ITO/10%-MCN/BiOI electrodes in on-off cycles under visible light irradiation were investigated and the results are shown in Figure 1c. The photocurrent intensity generated by 10%-MCN/BiOI electrode was about 1.5 and 2.0 times of those induced by BiOI and MCN under visible light irradiation, respectively. This result supports the hypothesis that the formation of heterojunction promotes faster charge separation and thus an increased photocurrent. The interface charge separation efficiency is an importance factor for photocatalytic performance, and was examined by EIS. The EIS Nyquist plots of MCN, BiOI and MCN/BiOI without and with irradiation are demonstrated in Figure 1d. A smaller arc radium in the EIS Nyquist plot implies a more effective separation of the photogenerated hole-electron pairs and a faster interfacial charge transfer.[38] Figure 1d illustrates that the impedance arc radius of 10%-MCN/BiOI was much smaller than pure MCN and BiOI under visible light irradiation, implying that the hybridization of MCN changed the charge distribution of BiOI and made charge transfer easier.[33] This further supports that the photogenerated electron-hole pairs were more effectively separated in the composite and there was a more efficient interfacial charge transfer between the electron donor and electron acceptor.

3.2. Characterization of Prepared Catalysts. Figure S2 in the Supporting Information presents the XRD patterns of MCN, BiOI, and MCN/BiOI composites. The peak at 27.4° in pure MCN reveals the graphite-like structure, and is indexed as (002) characteristic peak, corresponding to the interlayer stacking of conjugated aromatic systems.[12] The diffraction peaks of the prepared BiOI are consistent with that of JCPDS No. 73-2062, suggesting that pure BiOI crystal phase was formed. The XRD patterns of BiOI do not show significant change when it was hybridized with MCN, indicating that hybridization of MCN did not give rise to the development of new crystal orientations. The presence of MCN in the composites could be easily identified by Fourier transform infrared and XPS spectra, which will be discussed later.

The morphology and the microstructure of the prepared photocatalysts were characterized by FE-SEM and HR-TEM, as shown in Figure 2. As Figure 2a shows, the MCN exhibits an aggregated morphology and stacking pimple-like structure with a size of several micrometers resulting from the gases discharging from the thermal polycondensation of cyanamide ($CN\text{-}NH_2$). Figure 2b demonstrates that BiOI is mainly present as 3D hierarchical microspheres with an average diameter of 2-3 μm, which are assembled from two-dimensional nanosheets. After hybridization with the MCN polymer, the BiOI microspheres were well interwoven among MCN (Figure 2c), forming a 3D hybridized structure, which would facilitate the transfer of photogenerated carriers and improve the photocatalytic performance. The HR-TEM image of MCN/BiOI in Figure 2d reveals that a lattice spacing of MCN crystallites was 0.326 nm, corresponding to the interlayer structural packing indexed for the (002) crystallographic plane of hexagonal g-C_3N_4 [JCPDS No. 87-1526].[39] In addition, another lattice spacing was identified as 0.282 nm, which is characteristic of the (110) crystallographic plane of tetragonal BiOI [JCPDS No. 73-2062].[40] This indicates that a MCN/BiOI heterojunction between MCN (002) and BiOI (110) might be formed in the composite. In addition, the fast Fourier transform (FFT) patterns in Figure 2d (inset) further demonstrates the coexistence of hexagonal g-C_3N_4 and tetragonal BiOI, respectively.

The optical properties of BiOI, MCN, and MCN/BiOI were investigated by UV−vis diffuse reflectance spectra. As shown in Figure 3, BiOI presented strong photoabsorption from the UV light to visible light shorter than 632 nm. In comparison with it, the photoabsorption of MCN was weaker in the range of <600

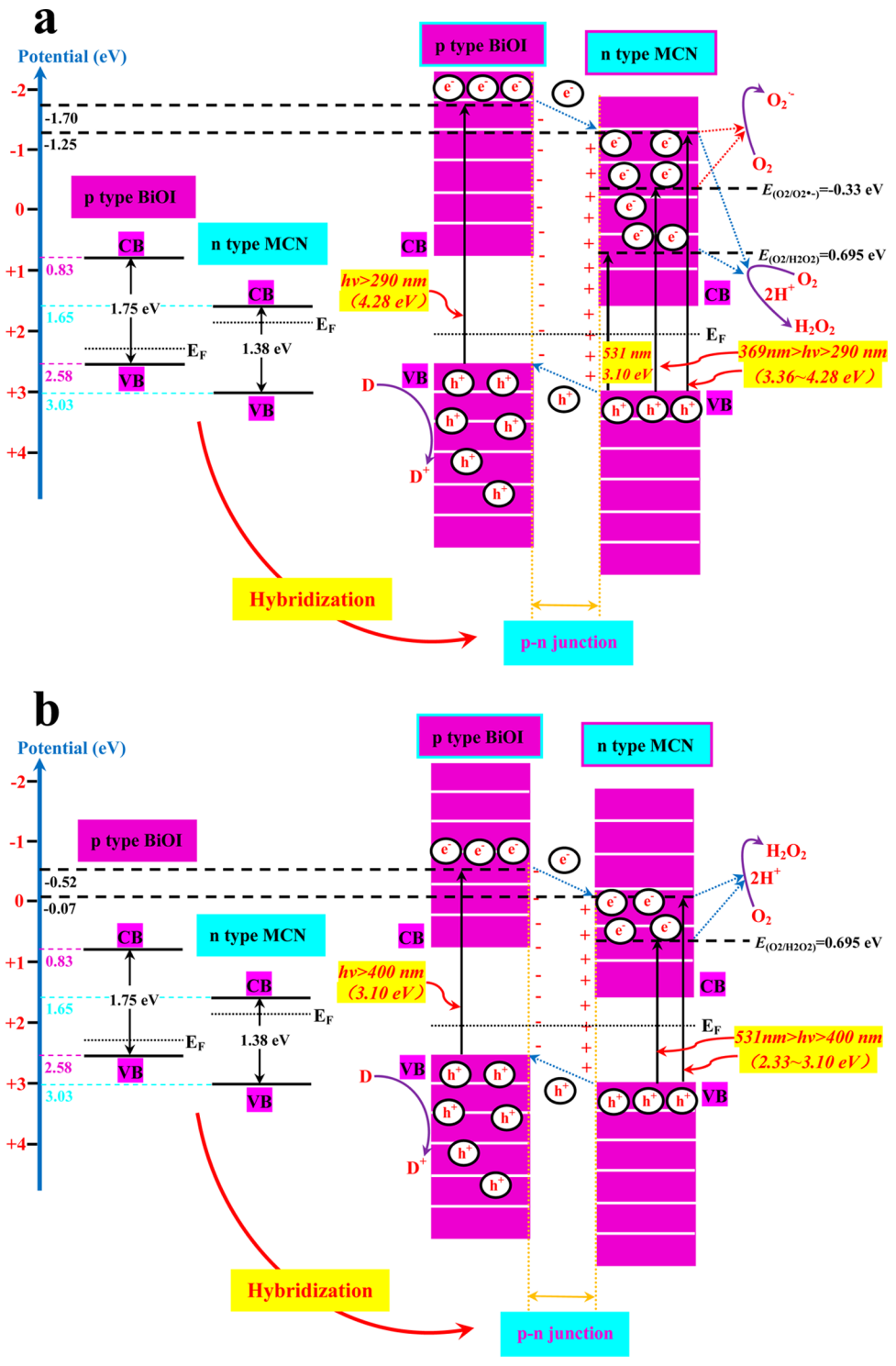

Figure 4. Schematic diagram of energy bands of p type BiOI and n type MCN and the transfer of photogenerated charges in the MCN/BiOI heterojunctions under (a) simulated solar light (λ > 290 nm) and (b) visible-light irradiation (λ > 400 nm).

nm, but displayed an absorption edge at about 735 nm, indicating a smaller band gap. Recently, Yan et al. also reported that mesoporous graphitic carbon nitride not only possessed high BET surface area but also exhibited redshift in absorbance edge up to 800 nm.[41] As BiOI was hybridized with MCN, the absorption edge of 10%-MCN/BiOI composite shifted red in the range of 600−1000 nm as compared to pure BiOI, whereas the absorption intensity in the visible light region was higher than that of pure MCN. For a crystalline semiconductor, the optical band gap could be calculated from the classic Tauc approach by using the following equation: $\alpha h\nu = A(h\nu - E_g)^{n/2}$,[42] where α, ν, E_g, and A are the absorption coefficient, light frequency, band gap, and a constant, respectively. In the equation, n is a number characteristics of the transition in a semiconductor (direct transition $n = 1$ and indirect transition $n = 4$). Therefore, E_g could be estimated from the intercept of a tangent to the plot. The energy band of

dx.doi.org/10.1021/am5002597 | ACS Appl. Mater. Interfaces 2014, 6, 5083−5093

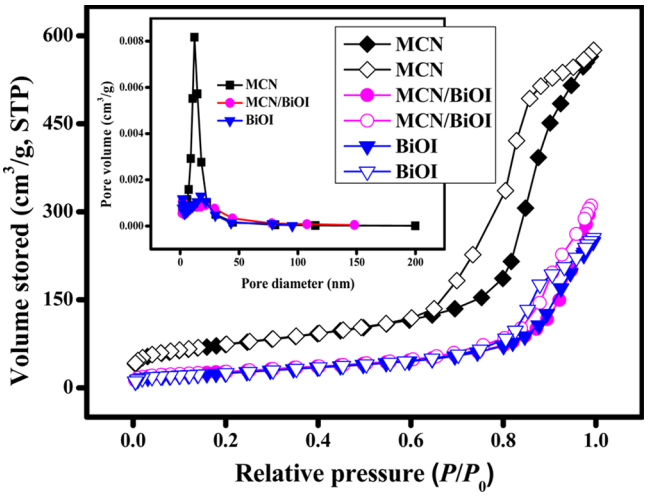

Figure 5. N_2 adsorption−desorption isotherms of the prepared materials. Closed symbols, adsorption; open symbols, desorption. Inset: Pore size distributions of the prepared materials.

MCN, BiOI, and 10%-MCN/BiOI was estimated according to the following empirical equations:[43]

$$E_{VB} = X - E^e + 0.5E_g \quad (2)$$

$$E_{CB} = E_{VB} - E_g \quad (3)$$

where E_{VB} and E_{CB} are the valence band (VB) and conduction band (CB) edge potentials, respectively; X is the geometric mean for absolute electronegativity of the constituent atoms (see Table 1a). The X values for MCN and BiOI are 6.84 and 6.21 eV, respectively. E^e is the energy of free electrons on the hydrogen scale (about 4.5 eV), and E_g is the band gap energy of the semiconductor. The energy band parameters of MCN and BiOI were calculated, and listed in Table 1b. For p-type BiOI, the Fermi level lies above its valence band whereas that of n-type MCN lies below its conduction band. When BiOI was hybridized by MCN, a p−n heterojunction would be formed and the charge carriers would diffuse in opposite direction to form an internal electric field with a direction from n-type MCN to p-type BiOI at the heterojunction interface, as shown in Figure 4. The Fermi levels of MCN and BiOI would be aligned under thermodynamic equilibrium conditions. Meanwhile, the energy band positions of MCN shifted downward and that of BiOI shifted upward along with the Fermi level.[3] Under simulated solar-light (λ > 290 nm) or visible-light irradiation (λ > 400 nm), BiOI and MCN could be simultaneously excited to generate electron-hole pairs. According to the band edge position, the excited electrons produced by BiOI were injected into the CB of MCN, while the photogenerated holes were effectively collected in the VB of BiOI. Because of the formation of internal electric field, the migration of photogenerated carriers was promoted.[44] Therefore, the photogenerated carriers could be effectively separated. This explains the results that the composites displayed higher photocatalytic and photoelectrochemical performance.

The N_2 adsorption/desorption isotherms are demonstrated in Figure 5. The isotherms of all measured samples were characteristic of type IV with a hysteresis loop observed in the range of 0.60-1.00 P/P_0, suggesting their mesoporous properties. The BET surface area (S_{BET}) of the MCN and pure BiOI was 243.2 and 88.7 $m^2\ g^{-1}$ respectively, while that of 10%-MCN/BiOI was 97.5 $m^2\ g^{-1}$, higher than pure BiOI but lower than pure MCN. From Table S1 in the Supporting Information, the S_{BET} of the composite catalysts increased gradually with increasing the proportion of MCN. In addition, the pore size distribution in Figure 5 (inset) shows that the pores of all measured samples were mainly distributed in the range of 0−50 nm, agreeing with the mesoporous structure. The BJH adsorption cumulative volume of pores increased from 0.37 to 0.47 $cm^3\ g^{-1}$ after MCN (0.87 $cm^3\ g^{-1}$) hybridization.

The FT-IR spectra of pristine MCN, MCN/BiOI and pure BiOI are demonstrated in Figure 6 to investigate their compositions and structures. In the spectrum of pristine MCN, the sharp peak at 808 cm^{-1} was attributed to the s-triazine ring modes, which is in accordance with previous studies.[27,30] The four peaks at 1250, 1325, 1420, and 1572 cm^{-1} observed in MCN are assigned to the typical stretching modes of CN heterocycle, whereas the peak at 1639 cm^{-1} could be assigned to the C═N stretching vibration mode.[34,39,45] A wide peak near 3175 cm^{-1} corresponds to the stretching mode of terminal NH groups at the defect sites of the aromatic ring,[45] whereas the sharp peak at 2180 cm^{-1} corresponds to the stretching mode of CN structure (C≡N).[46,47] After the hybridization of MCN and BiOI, the intensity of these peaks increased gradually with the increase of MCN content from 2

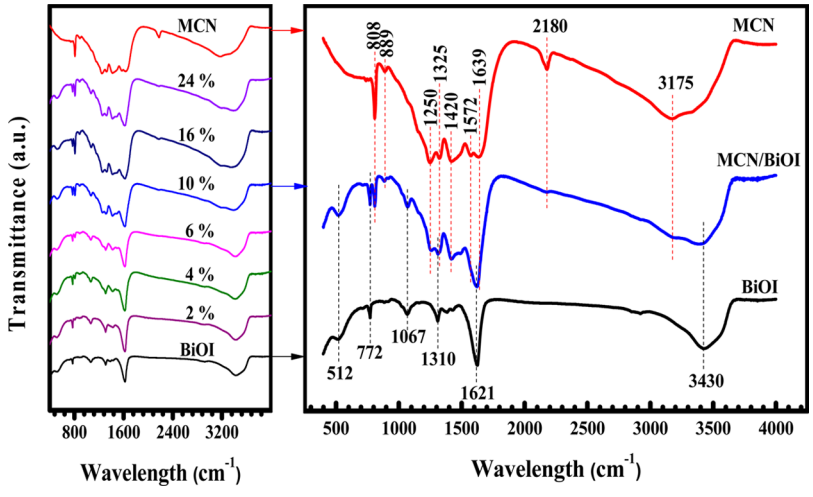

Figure 6. FT-IR spectra of the prepared materials.

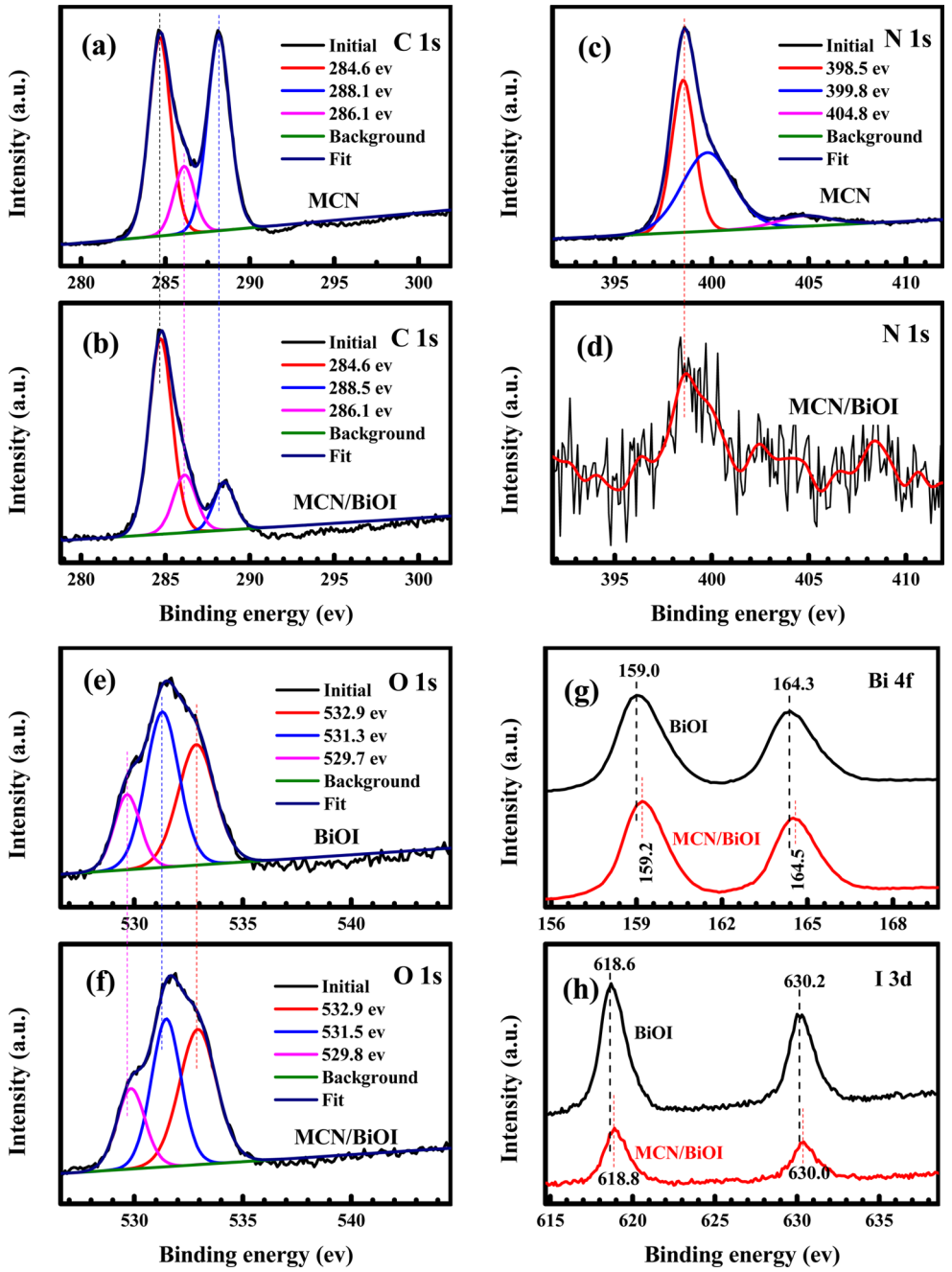

Figure 7. XPS spectra for: C 1s of (a) MCN and (b) MCN/BiOI; N 1s of (c) MCN and (d) MCN/BiOI; O 1s of (e) BiOI and (f) MCN/BiOI; (g) Bi 4f of BiOI and MCN/BiOI; and (h) I 3d of BiOI and MCN/BiOI. Note: all MCN/BiOI with MCN loading of 10%.

to 24%, indicating the successful incorporation of MCN in the MCN/BiOI composites. For pure BiOI, a peak at 512 cm^{-1} in the spectrum corresponding to symmetrical A_{2u}-type vibration of the Bi−O bond was observed, and is consistent with the published results.[40,48] The absorption at 772 cm^{-1} was assigned to the asymmetrical stretching vibration of Bi−O bond.[49,50] In addition, the presence of the sharp and strong absorption at 1621 cm^{-1} and a broad peak at 3430 cm^{-1} were ascribed to the δ(O−H) bending vibration and ν(O−H) stretching respectively due to the adsorption of free water molecules on the photocatalyst surface.[2] It is obvious that the main characteristic peaks of MCN and BiOI are almost present in all the MCN/BiOI composites.

To further elucidate the interaction between MCN and BiOI, we conducted XPS analysis to investigate the chemical states. Figure 7 illustrates the XPS spectra of C1s and N1s for pristine MCN and MCN/BiOI composites, as well as the O1s, Bi4f and I3d spectra for pure BiOI and the composites. Panels a and b in Figure 7 demonstrate that the C1s spectrum for both pure MCN and the composite can be fitted with three components. The component at 284.6 eV corresponded to C−C, which originated from pure graphitic carbon presumably formed during minor decomposition of the carbon nitride.[51] The other two peaks were attributed to C═N or C≡N originating from the defect-containing sp^2-hybridized carbon atoms present in graphitic domains,[47,52] and the sp^2-hybridized carbon in N═C−N_2 coordination, which connected with three neighboring

dx.doi.org/10.1021/am5002597 | ACS Appl. Mater. Interfaces 2014, 6, 5083−5093

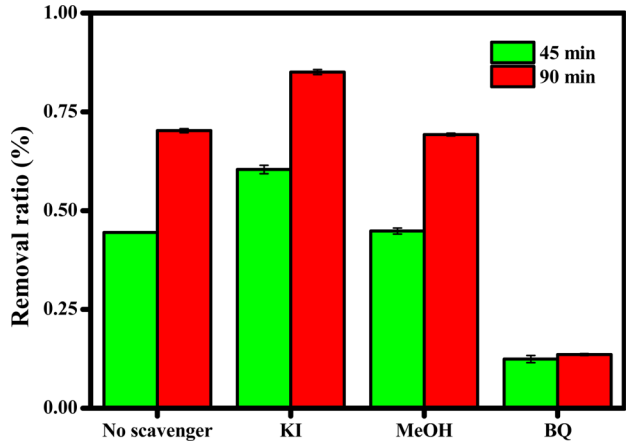

Figure 8. Effects of different reactive species scavengers on the photodegradation of BPA by 10%-MCN/BiOI under simulated solar light irradiation.

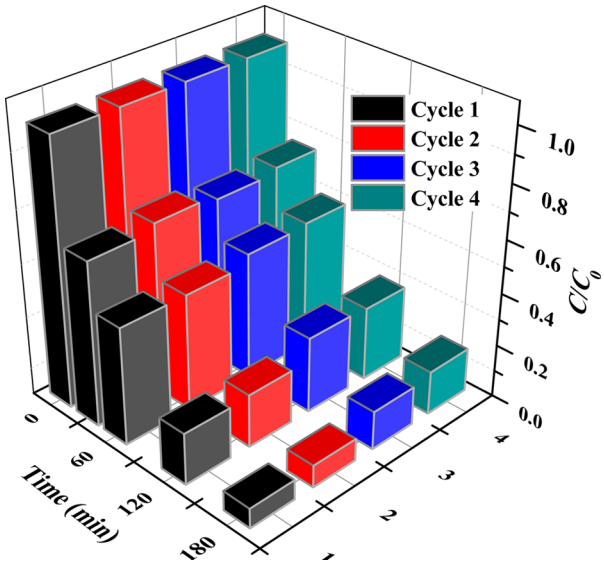

Figure 9. Recycling tests of 10%-MCN/BiOI under simulated solar light irradiation.

N atoms in one double and two single bonds,[53] respectively. After hybridization, the peak at 288.1 eV for pure MCN shifted to 288.5 eV and the intensity decreased significantly. In the N1s spectra (Figure 7c, d), the peak at 398.6 eV is typically ascribed to the nitrogen atoms sp^2-hybridized to two carbon atoms (C═N−C).[22] Because of the low proportion of MCN, the peak of N1s of the composite was weak. The XPS of N1s in the composite could be separated into three binding energies. Except for the predominant characteristic peak at 398.6 eV, the peak at 399.8 eV was ascribed to the tertiary nitrogen N—$(C)_3$ groups[54] while the last peak at 404.8 eV might be resulted from π-excitation.[53] The O1s spectra in panels e and f in Figure 7 consisted of three components: the peak at 529.7 eV was attributed to the Bi−O bonds in $[Bi_2O_2]$ slabs of BiOI[6] and the peak at 531.3 eV originated from I−O bonds in BiOI,[55] which shifted toward high energy after hybridizing with MCN, whereas the peak at 532.9 eV suggests the presence of other components such as OH, H_2O, and O_2 adsorbed on the surface.[6,56] The peaks of Bi $4f_{7/2}$ and Bi $4f_{5/2}$ were observed at 159.0 and 164.3 eV (Figure 7g), respectively, which are the characteristic of Bi^{3+} ions in BiOI.[4,5] However, the peaks Bi $4f_{7/2}$ and Bi $4f_{5/2}$ for MCN/BiOI composite at 159.2 and 164.5 eV are higher than those of pure BiOI. The I 3d XPS spectra in Fig. 7h could be observed at binding energies of 618.6 eV (I $3d_{5/2}$) and 630.0 eV (I $3d_{3/2}$) corresponding to I^- in BiOI.[4] A positive shift in the I^- binding energies was also observed when BiOI was hybridized by MCN. These results also imply that heterojunction exist between MCN and BiOI, not a simply physical adsorption. This interaction is essential for photogenerated charge carriers transfer and enhancing photocatalytic performance.

3.3. Photocatalytic Mechanisms of MCN/BiOI. The active species contributing to the oxidative reaction that were generated from the light irradiation progress were investigated by adding different scavengers, and the results are shown in Figure 8. The photocatalytic performance was enhanced with addition of KI as scavenger for photogenerated hole in the solution,[57,58] implying that scavenging h^+ might improve the electron-hole separation and increase the amount of free electrons, generating more active radicals such as hydroxyl radicals (•OH) and superoxide radical species ($O_2^{\bullet-}$ and $HO_2^{\bullet-}$).[59] However, the photocatalytic performance of MCN/BiOI did not change with the addition of CH_3OH as scavenger for •OH,[60] indicating that it was not the major oxidative species in the photocatalytic reaction system of MCN/BiOI. When BQ, which is a scavenger for superoxide radical species,[61] was added in the reaction system, the photocatalytic reaction was significantly inhibited. These results indicate that superoxide radicals might be a predominant active species responsible for the photocatalytic reaction. It is interesting that the conduction band edge (+1.65 eV vs. NHE) of MCN is more positive than the redox of superoxide radical formation: $E(O_2/O_2^{\bullet-}) = -0.33$ eV vs. NHE.[62] However, the electrons in the valence band of MCN could be excited up to a higher potential edge (−0.33 to −1.25 eV) under simulated solar light irradiation with energy 3.36−4.28 eV (369 nm > λ > 290 nm), and the reformed conduction band electrons of MCN could reduce O_2 to $O_2^{\bullet-}$ and $HO_2^{\bullet-}$ (from Figure 4a). It is reported that superoxide radicals, such as $O_2^{\bullet-}$ and $HO_2^{\bullet-}$, are very active radicals for the ring cleavage of aromatic compounds.[63] Under visible-light irradiation with energy 2.33−3.10 eV (531 nm > λ > 400 nm), the electrons in the valence band of MCN could be excited up to a higher potential edge (0.695 to −0.07 eV). The reformed conduction band electrons of MCN could reduce O_2 to H_2O_2 by equation $O_2 + 2H^+ + 2e^- \rightarrow H_2O_2$ (0.695 eV vs. NHE[64]) as shown in Figure 4b. An et al. also confirm that H_2O_2 is strongly involved in the photocatalytic oxidation process.[65,66]

3.4. Stability of MCN/BiOI Photocatalyst. The recycle experiments of the MCN/BiOI for photocatalytic reaction under simulated solar light was investigated to evaluate the optical stability of the catalyst and the results are shown in Figure 9. The MCN/BiOI did not exhibit significant loss of photocatalytic performance after four recycling runs, and about 83.6% of BPA could be degraded after four runs. The results indicate that MCN/BiOI keeps its photocatalytic performance without distinct photocorrosion during the oxidation of pollutant. In addition, the XRD pattern of the 10%-MCN/BiOI after four times reuse is shown in Figure S3 in the Supporting Information. No significant differences in the diffraction peaks were observed, indicating that the composite of 10%-MCN/BiOI has a very stable crystal structure. These results suggest that the composite of 10%-MCN/BiOI displays very good stability and could be reused as a photocatalyst.

dx.doi.org/10.1021/am5002597 | ACS Appl. Mater. Interfaces 2014, 6, 5083−5093

4. CONCLUSIONS

BiOI was successfully hybridized with mesoporous graphite-like carbon nitride by a facile solvothermal method. The heterojunction structure of n-type MCN and p-type BiOI promoted the photogenerated charge separation, and hence the photocatalytic performance of BiOI was enhanced for the degradation of BPA under both visible light and simulated solar light irradiation. The composite with 10% MCN displayed the highest photocatalytic performance, and about 90.0% of BPA (20 mg L^{-1}) was photodegraded by the solids of 1.0 g L^{-1} 10%-MCN/BiOI after irradiation with visible light for 240 min.

■ ASSOCIATED CONTENT

Supporting Information

Materials and reagents, the synthesis method of MCN, the characterization methods of photocatalysts, the instrumental analysis method of BPA, and the additional XRD results of the prepared materials. This material is free of charge via the internet at http://pubs.acs.org.

■ AUTHOR INFORMATION

Corresponding Author

* E-mail: zhuly@nankai.edu.cn. Tel.: +86 22 23500791. Fax: +86 22 23508807.

Notes

The authors declare no competing financial interest.

■ ACKNOWLEDGMENTS

The authors gratefully acknowledge the financial support of Ministry of Science and Technology (2014CB932001, 2012ZX07529-003), Tianjin Municipal Science and Technology Commission (13JCZDJC35900), and the Fundamental Research Funds for the Central Universities.

■ REFERENCES

(1) Pan, C.; Xu, J.; Wang, Y.; Li, D.; Zhu, Y. Dramatic Activity of $C_3N_4/BiPO_4$ Photocatalyst with Core/Shell Structure Formed by Self-Assembly. *Adv. Funct. Mater.* **2012**, *22*, 1518−1524.

(2) Cao, J.; Xu, B.; Lin, H.; Luo, B.; Chen, S. Novel Heterostructured $Bi_2S_3/BiOI$ Photocatalyst: Facile Preparation, Characterization and Visible Light Photocatalytic Performance. *Dalton Trans.* **2012**, *41*, 11482−11490.

(3) Reddy, K. H.; Martha, S.; Parida, K. M. Fabrication of Novel p-BiOI/n-$ZnTiO_3$ Heterojunction for Degradation of Rhodamine 6G under Visible Light Irradiation. *Inorg. Chem.* **2013**, *52*, 6390−6401.

(4) Liu, H.; Cao, W. R.; Su, Y.; Wang, Y.; Wang, X. H. Synthesis, Characterization and Photocatalytic Performance of Novel Visible-Light-Induced Ag/BiOI. *Appl. Catal., B* **2012**, *111*, 271−279.

(5) Dai, G. P.; Yu, J. G.; Liu, G. Synthesis and Enhanced Visible-Light Photoelectrocatalytic Activity of P−N Junction $BiOI/TiO_2$ Nanotube Arrays. *J. Phys. Chem. C* **2011**, *115*, 7339−7346.

(6) Jiang, J.; Zhang, X.; Sun, P. B.; Zhang, L. Z. ZnO/BiOI Heterostructures: Photoinduced Charge-Transfer Property and Enhanced Visible-Light Photocatalytic Activity. *J. Phys. Chem. C* **2011**, *115*, 20555−20564.

(7) Li, H. Q.; Cui, Y. M.; Hong, W. S. High Photocatalytic Performance of $BiIO/Bi_2WO_6$ toward Toluene and Reactive Brilliant Red. *Appl. Surf. Sci.* **2013**, *264*, 581−588.

(8) Cheng, H. F.; Huang, B. B.; Dai, Y.; Qin, X. Y.; Zhang, X. Y. One-Step Synthesis of the Nanostructured AgI/BiOI Composites with Highly Enhanced Visible-Light Photocatalytic Performances. *Langmuir* **2010**, *26*, 6618−6624.

(9) Yu, J.; Wang, S.; Cheng, B.; Lin, Z.; Huang, F. Noble Metal-Free $Ni(OH)_2$-g-C_3N_4 Composite Photocatalyst with Enhanced Visible-Light Photocatalytic H_2-Production Activity. *Catal. Sci. Technol.* **2013**, *3*, 1782−1789.

(10) Kumar, S.; Surendar, T.; Baruah, A.; Shanker, V. Synthesis of a Novel and Stable g-C_3N_4-Ag_3PO_4 Hybrid Nanocomposite Photocatalyst and Study of the Photocatalytic Activity under Visible Light Irradiation. *J. Mater. Chem. A* **2013**, *1*, 5333−5340.

(11) Wang, X. C.; Maeda, K.; Thomas, A.; Takanabe, K.; Xin, G.; Carlsson, J. M.; Domen, K.; Antonietti, M. A Metal-Free Polymeric Photocatalyst for Hydrogen Production from Water under Visible Light. *Nat. Mater.* **2009**, *8*, 76−80.

(12) Groenewolt, M.; Antonietti, M. Synthesis of g-C_3N_4 Nanoparticles in Mesoporous Silica Host Matrices. *Adv. Mater.* **2005**, *17*, 1789−1792.

(13) Bai, X.; Wang, L.; Zong, R.; Zhu, Y. Photocatalytic Activity Enhanced Via g-C_3N_4 Nanoplates to Nanorods. *J. Phys. Chem. C* **2013**, *117*, 9952−9961.

(14) Wang, Y.; Zhang, J. S.; Wang, X. C.; Antonietti, M.; Li, H. R. Boron- and Fluorine-Containing Mesoporous Carbon Nitride Polymers: Metal-Free Catalysts for Cyclohexane Oxidation. *Angew. Chem., Int. Ed.* **2010**, *49*, 3356−3359.

(15) Wang, Y.; Li, H. R.; Yao, J.; Wang, X. C.; Antonietti, M. Synthesis of Boron Doped Polymeric Carbon Nitride Solids and Their Use as Metal-Free Catalysts for Aliphatic C−H Bond Oxidation. *Chem. Sci.* **2011**, *2*, 446−450.

(16) Wang, Y.; Di, Y.; Antonietti, M.; Li, H. R.; Chen, X. F.; Wang, X. C. Excellent Visible-Light Photocatalysis of Fluorinated Polymeric Carbon Nitride Solids. *Chem. Mater.* **2010**, *22*, 5119−5121.

(17) Zhang, Y. J.; Mori, T.; Ye, J. H.; Antonietti, M. Phosphorus-Doped Carbon Nitride Solid: Enhanced Electrical Conductivity and Photocurrent Generation. *J. Am. Chem. Soc.* **2010**, *132*, 6294−6295.

(18) Liu, G.; Niu, P.; Sun, C.; Smith, S. C.; Chen, Z.; Lu, G. Q.; Cheng, H.-M. Unique Electronic Structure Induced High Photoreactivity of Sulfur-Doped Graphitic C_3N_4. *J. Am. Chem. Soc.* **2010**, *132*, 11642−11648.

(19) Zhang, J. S.; Sun, J. H.; Maeda, K.; Domen, K.; Liu, P.; Antonietti, M.; Fu, X. Z.; Wang, X. C. Sulfur-Mediated Synthesis of Carbon Nitride: Band-Gap Engineering and Improved Functions for Photocatalysis. *Energy Environ. Sci.* **2011**, *4*, 675−678.

(20) Wang, X. C.; Chen, X. F.; Thomas, A.; Fu, X. Z.; Antonietti, M. Metal-Containing Carbon Nitride Compounds: A New Functional Organic-Metal Hybrid Material. *Adv. Mater.* **2009**, *21*, 1609−1612.

(21) Chen, X. F.; Zhang, J. S.; Fu, X. Z.; Antonietti, M.; Wang, X. C. Fe-g-C_3N_4-Catalyzed Oxidation of Benzene to Phenol Using Hydrogen Peroxide and Visible Light. *J. Am. Chem. Soc.* **2009**, *131*, 11658−11659.

(22) Ding, Z. X.; Chen, X. F.; Antonietti, M.; Wang, X. C. Synthesis of Transition Metal-Modified Carbon Nitride Polymers for Selective Hydrocarbon Oxidation. *Chemsuschem* **2011**, *4*, 274−281.

(23) Wang, Y.; Yao, J.; Li, H. R.; Su, D. S.; Antonietti, M. Highly Selective Hydrogenation of Phenol and Derivatives over a Pd@Carbon Nitride Catalyst in Aqueous Media. *J. Am. Chem. Soc.* **2011**, *133*, 2362−2365.

(24) Ghosh, K.; Kumar, M.; Wang, H. F.; Maruyama, T.; Ando, Y. Facile Decoration of Platinum Nanoparticles on Carbon-Nitride Nanotubes Via Microwave-Assisted Chemical Reduction and Their Optimization for Field-Emission Application. *J. Phys. Chem. C* **2010**, *114*, 5107−5112.

(25) Datta, K. K. R.; Reddy, B. V. S.; Ariga, K.; Vinu, A. Gold Nanoparticles Embedded in a Mesoporous Carbon Nitride Stabilizer for Highly Efficient Three-Component Coupling Reaction. *Angew. Chem., Int. Ed.* **2010**, *49*, 5961−5965.

(26) Zhou, X.; Jin, B.; Li, L.; Peng, F.; Wang, H.; Yu, H.; Fang, Y. A Carbon Nitride/TiO_2 Nanotube Array Heterojunction Visible-Light Photocatalyst: Synthesis, Characterization, and Photoelectrochemical Properties. *J. Mater. Chem.* **2012**, *22*, 17900−17905.

(27) Wang, Y.; Shi, R.; Lin, J.; Zhu, Y. Enhancement of Photocurrent and Photocatalytic Activity of ZnO Hybridized with Graphite-Like C_3N_4. *Energy Environ. Sci.* **2011**, *4*, 2922−2929.

(28) Sun, J.-X.; Yuan, Y.-P.; Qiu, L.-G.; Jiang, X.; Xie, A.-J.; Shen, Y.-H.; Zhu, J.-F. Fabrication of Composite Photocatalyst g-C_3N_4-ZnO and Enhancement of Photocatalytic Activity under Visible Light. *Dalton Trans.* **2012**, *41*, 6756−6763.
(29) Hong, J.; Wang, Y.; Wang, Y.; Zhang, W.; Xu, R. Noble-Metal-Free NiS/C_3N_4 for Efficient Photocatalytic Hydrogen Evolution from Water. *ChemSusChem* **2013**, *6*, 2263−2268.
(30) Sun, L.; Zhao, X.; Jia, C.-J.; Zhou, Y.; Cheng, X.; Li, P.; Liu, L.; Fan, W. Enhanced Visible-Light Photocatalytic Activity of g-C_3N_4-$ZnWO_4$ by Fabricating a Heterojunction: Investigation Based on Experimental and Theoretical Studies. *J. Mater. Chem.* **2012**, *22*, 23428−23438.
(31) Wang, Y.; Wang, Z.; Muhammad, S.; He, J. Graphite-Like C_3N_4 Hybridized $ZnWO_4$ Nanorods: Synthesis and Its Enhanced Photocatalysis in Visible Light. *Crystengcomm* **2012**, *14*, 5065−5070.
(32) Ge, L.; Han, C. C.; Liu, J. Novel Visible Light-Induced g-C_3N_4/Bi_2WO_6 Composite Photocatalysts for Efficient Degradation of Methyl Orange. *Appl. Catal., B* **2011**, *108*, 100−107.
(33) Wang, Y. J.; Bai, X. J.; Pan, C. S.; He, J.; Zhu, Y. F. Enhancement of Photocatalytic Activity of Bi_2WO_6 Hybridized with Graphite-Like C_3N_4. *J. Mater. Chem.* **2012**, *22*, 11568−11573.
(34) Fu, J.; Tian, Y.; Chang, B.; Xi, F.; Dong, X. BiOBr-Carbon Nitride Heterojunctions: Synthesis, Enhanced Activity and Photocatalytic Mechanism. *J. Mater. Chem.* **2012**, *22*, 21159−21166.
(35) Li, J.; Lu, G.; Wang, Y.; Guo, Y.; Guo, Y. A High Activity Photocatalyst of Hierarchical 3D Flowerlike ZnO Microspheres: Synthesis, Characterization and Catalytic Activity. *J. Colloid Interface Sci.* **2012**, *377*, 191−196.
(36) Xiao, X.; Hao, R.; Liang, M.; Zuo, X. X.; Nan, J. M.; Li, L. S.; Zhang, W. D. One-Pot Solvothermal Synthesis of Three-Dimensional (3D) BiOI/BiOCl Composites with Enhanced Visible-Light Photocatalytic Activities for the Degradation of Bisphenol-A. *J. Hazard. Mater.* **2012**, *233*, 122−130.
(37) Goettmann, F.; Fischer, A.; Antonietti, M.; Thomas, A. Chemical Synthesis of Mesoporous Carbon Nitrides Using Hard Templates and Their Use as a Metal-Free Catalyst for Friedel-Crafts Reaction of Benzene. *Angew. Chem.,. Int. Ed.* **2006**, *45*, 4467−4471.
(38) Xiao, F. X.; Wang, F. C.; Fu, X. Z.; Zheng, Y. A Green and Facile Self-Assembly Preparation of Gold Nanoparticles/Zno Nanocomposite for Photocatalytic and Photoelectrochemical Applications. *J. Mater. Chem.* **2012**, *22*, 2868−2877.
(39) Ge, L.; Zuo, F.; Liu, J.; Ma, Q.; Wang, C.; Sun, D.; Bartels, L.; Feng, P. Synthesis and Efficient Visible Light Photocatalytic Hydrogen Evolution of Polymeric g-C_3N_4 Coupled with CdS Quantum Dots. *J. Phys. Chem. C* **2012**, *116*, 13708−13714.
(40) Wang, Y. N.; Deng, K. J.; Zhang, L. Z. Visible Light Photocatalysis of BiOI and Its Photocatalytic Activity Enhancement by in Situ Ionic Liquid Modification. *J. Phys. Chem. C* **2011**, *115*, 14300−14308.
(41) Yan, H. Soft-Templating Synthesis of Mesoporous Graphitic Carbon Nitride with Enhanced Photocatalytic H_2 Evolution under Visible Light. *Chem. Commun.* **2012**, *48*, 3430−3432.
(42) Ma, H.; Shen, J.; Shi, M.; Lu, X.; Li, Z.; Long, Y.; Li, N.; Ye, M. Significant Enhanced Performance for Rhodamine B, Phenol and Cr(VI) Removal by Bi_2WO_6 Nancomposites Via Reduced Graphene Oxide Modification. *Appl. Catal., B* **2012**, *121−122*, 198−205.
(43) Li, Y.; Wang, J.; Yao, H.; Dang, L.; Li, Z. Chemical Etching Preparation of BiOI/Bi_2O_3 Heterostructures with Enhanced Photocatalytic Activities. *Catal. Commun.* **2011**, *12*, 660−664.
(44) Long, M.; Cai, W.; Cai, J.; Zhou, B.; Chai, X.; Wu, Y. Efficient Photocatalytic Degradation of Phenol over Co_3O_4/$BiVO_4$ Composite under Visible Light Irradiation. *J. Phys. Chem. B* **2006**, *110*, 20211−20216.
(45) Chai, B.; Peng, T.; Mao, J.; Li, K.; Zan, L. Graphitic Carbon Nitride (g-C_3N_4)-Pt-TiO_2 Nanocomposite as an Efficient Photocatalyst for Hydrogen Production under Visible Light Irradiation. *Phys. Chem. Chem. Phys.* **2012**, *14*, 16745−16752.
(46) Bojdys, M. J.; Muller, J. O.; Antonietti, M.; Thomas, A. Ionothermal Synthesis of Crystalline, Condensed, Graphitic Carbon Nitride. *Chem.—Eur. J.* **2008**, *14*, 8177−8182.
(47) Lei, W.; Portehault, D.; Dimova, R.; Antoniettit, M. Boron Carbon Nitride Nanostructures from Salt Melts: Tunable Water-Soluble Phosphors. *J. Am. Chem. Soc.* **2011**, *133*, 7121−7127.
(48) Wang, C. H.; Shao, C. L.; Liu, Y. C.; Zhang, L. Photocatalytic Properties Biocl and Bi_2O_3 Nanofibers Prepared by Electrospinning. *Scr. Mater.* **2008**, *59*, 332−335.
(49) Gurunathan, K. Photocatalytic Hydrogen Production Using Transition Metal Ions-Doped γ-Bi_2O_3 Semiconductor Particles. *Int. J. Hydrogen Energy* **2004**, *29*, 933−940.
(50) Liu, Z.; Xu, X. X.; Fang, J. Z.; Zhu, X. M.; Chu, J. H.; Li, B. J. Microemulsion Synthesis, Characterization of Bismuth Oxyiodine/Titanium Dioxide Hybrid Nanoparticles with Outstanding Photocatalytic Performance under Visible Light Irradiation. *Appl. Surf. Sci.* **2012**, *258*, 3771−3778.
(51) Khabashesku, V. N.; Zimmerman, J. L.; Margrave, J. L. Powder Synthesis and Characterization of Amorphous Carbon Nitride. *Chem. Mater.* **2000**, *12*, 3264−3270.
(52) Xiang, Q. J.; Yu, J. G.; Jaroniec, M. Preparation and Enhanced Visible-Light Photocatalytic H_2 Production Activity of Graphene/C_3N_4 Composites. *J. Phys. Chem. C* **2011**, *115*, 7355−7363.
(53) Guo, Q. X.; Xie, Y.; Wang, X. J.; Zhang, S. Y.; Hou, T.; Lv, S. C. Synthesis of Carbon Nitride Nanotubes with the C_3N_4 Stoichiometry Via a Benzene-Thermal Process at Low Temperatures. *Chem. Commun.* **2004**, 26−27.
(54) Dementjev, A. P.; de Graaf, A.; van de Sanden, M. C. M.; Maslakov, K. I.; Naumkin, A. V.; Serov, A. A. X-Ray Photoelectron Spectroscopy Reference Data for Identification of the C_3N_4 Phase in Carbon−Nitrogen Films. *Diamond Relat. Mater.* **2000**, *9*, 1904−1907.
(55) Yu, C. L.; Yu, J. C.; Fan, C. F.; Wen, H. R.; Hu, S. J. Synthesis and Characterization of Pt/BiOI Nanoplate Catalyst with Enhanced Activity under Visible Light Irradiation. *Mater. Sci. Eng., B* **2010**, *166*, 213−219.
(56) Bi, J.; Wu, L.; Li, Z.; Ding, Z.; Wang, X.; Fu, X. A Facile Microwave Solvothermal Process to Synthesize $ZnWO_4$ Nanoparticles. *J. Alloys Compd.* **2009**, *480*, 684−688.
(57) Van Doorslaer, X.; Heynderickx, P. M.; Demeestere, K.; Debevere, K.; Van Langenhove, H.; Dewulf, J. TiO_2 Mediated Heterogeneous Photocatalytic Degradation of Moxifloxacin: Operational Variables and Scavenger Study. *Appl. Catal., B* **2012**, *111−112*, 150−156.
(58) An, T.; An, J.; Yang, H.; Li, G.; Feng, H.; Nie, X. Photocatalytic Degradation Kinetics and Mechanism of Antivirus Drug-Lamivudine in TiO_2 Dispersion. *J. Hazard. Mater.* **2011**, *197*, 229−236.
(59) Chang, C.; Fu, Y.; Hu, M.; Wang, C.; Shan, G.; Zhu, L. Photodegradation of Bisphenol A by Highly Stable Palladium-Doped Mesoporous Graphite Carbon Nitride (Pd/mpg-C_3N_4) under Simulated Solar Light Irradiation. *Appl. Catal., B* **2013**, *142−143*, 553−560.
(60) Hazime, R.; Ferronato, C.; Fine, L.; Salvador, A.; Jaber, F.; Chovelon, J. M. Photocatalytic Degradation of Imazalil in an Aqueous Suspension of TiO_2 and Influence of Alcohols on the Degradation. *Appl. Catal., B* **2012**, *126*, 90−99.
(61) Zhang, Y.; Zhang, N.; Tang, Z.-R.; Xu, Y.-J. Transforming CdS into an Efficient Visible Light Photocatalyst for Selective Oxidation of Saturated Primary C−H Bonds under Ambient Conditions. *Chem. Sci.* **2012**, *3*, 2812−2822.
(62) Teoh, W. A Perspective on the Flame Spray Synthesis of Photocatalyst Nanoparticles. *Materials* **2013**, *6*, 3194−3212.
(63) Ng, J. W.; Wang, X. P.; Sun, D. D. One-Pot Hydrothermal Synthesis of a Hierarchical Nanofungus-Like Anatase TiO_2 Thin Film for Photocatalytic Oxidation of Bisphenol A. *Appl. Catal., B* **2011**, *110*, 260−272.
(64) Tian, L.; Liu, J.; Gong, C.; Ye, L.; Zan, L. Fabrication of Reduced Graphene Oxide−BiOCl Hybrid Material Via a Novel Benzyl Alcohol Route and Its Enhanced Photocatalytic Activity. *J. Nanopart. Res.* **2013**, *15*, 1−11.

(65) Chen, Y.; Lu, A.; Li, Y.; Zhang, L.; Yip, H. Y.; Zhao, H.; An, T.; Wong, P.-K. Naturally Occurring Sphalerite as a Novel Cost-Effective Photocatalyst for Bacterial Disinfection under Visible Light. *Environ. Sci. Technol.* **2011**, *45*, 5689−5695.
(66) Fang, H.; Gao, Y.; Li, G.; An, J.; Wong, P.-K.; Fu, H.; Yao, S.; Nie, X.; An, T. Advanced Oxidation Kinetics and Mechanism of Preservative Propylparaben Degradation in Aqueous Suspension of TiO_2 and Risk Assessment of Its Degradation Products. *Environ. Sci. Technol.* **2013**, *47*, 2704−2712.